A Sampler Designed for Nanoparticles and Respirable Particles with Direct Analysis Feature

Candace Su-Jung Tsai[1]*, Daniel Theisen[1]

[1]Department of Environmental & Radiological Health Sciences, College of Veterinary Medicine & Biomedical Sciences, Colorado State University, 80523 CO

Corresponding author:

*Prof. Candace S.J. Tsai

1681 Campus Delivery, EH Room 153, Fort Collins CO, 80523-1681

Candace.Tsai@colostate.edu

Office: +1 (970) 491-1340

Fax: +1 (970) 491-2940

Keywords: nanoparticle, sampler, diffusion, respirable, personal sampling, microscope analysis

Word count: 4553 Introduction to Acknowledgement. 7 figures and 2 tables.

A Sampler Designed for Nanoparticles and Respirable Particles with Direct Analysis Feature

ABSTRACT

A sampler has been designed to collect particles in the nanometer and respirable sizes directly onto a membrane filter and transmission electron microscopy (TEM) grid. The novel design aspects of this sampler include the selection of the diameter of the inlet probe, geometry of the sampler and the resulting air flow to the sampler, which together control the cutoff diameter which was determined experimentally to be a mass median aerodynamic diameter (MMAD) of 3.8 µm. The maximum aerodynamic diameter entering the sampler is designed to be approximately 8 µm. Nanometer sized particles are collected on both the filter and grid through diffusion, as confirmed by testing with aluminum oxide engineered nanoparticles collected on the filter which measured a count median diameter (CMD) of 500 nm and a geometric standard deviation (GSD) of 1.97. The primary particles and small agglomerates collected on the grid have a CMD of 100 nm and GSD of 2.3. This diffusion sampler collected close to, if not 100%, of the particles entering the sampler. The sampler is easily wearable, operates at 0.3 L/min and efficiently collected particles in various settings. Particles are analyzed directly by transmission electron microscope on the grid and by scanning electron microscope on the filter to assess the exposure through particle counts and elemental composition analysis.

INTRODUCTION

Due to the greater awareness of potential harm by nanomaterials (Fleischer and Grunwald 2007; Maynard 2007; NSTC 2006; Oberdörster 2004; Roco 2003; Roco 2011; Schulte et al. 2008; Simeonova et al. 2007; Singh and Nalwa 2007; Warheit et al. 2008), the number of studies

investigating toxicological effects of nanomaterials has increased greatly in recent years. The risk of potential harm to the environment and humans from selected nanomaterials has been studied and concerns have been raised (Cena and Peters 2011; Dahm et al. 2012; Methner et al. 2007; Park et al. 2009; Tsai 2013; Tsai et al. 2009a; Tsai et al. 2008; Tsai et al. 2009b; Tsai et al. 2010). Airborne nanomaterials can expose humans through inhalation, and such nanoparticle exposures are typically assessed using some form of particle sampler.

Size selective sampling is critical to separate nanoparticles from large particles for collection. The traditional respirable filter sampler relies on a nylon cyclone to pre-separate particles in the respirable size range in order to measure respirable mass exposure. Aerosol particles frequently have a net charge; Briant and Moss (Briant and Moss 1984) found that if the cyclone itself has a net charge, particles with the same charge will be repelled by the electric field created around the cyclone body and be repelled from the cyclone inlet, decreasing their sampling efficiency and underestimating respirable mass. This issue will profoundly affect measurements of nanoparticles.

Several samplers designed to collect nanoparticles have become available since 2010, including the electrostatic precipitation sampler (ESP) (Miller et al. 2010), thermophoretic sampler (TPS) (Leith et al. 2014), personal nanoparticle sampler (PENS) (Tsai et al. 2012), and nanoparticle respiratory deposition (NRD) sampler (Cena et al. 2011), which use various particle deposition mechanisms including electrostatic precipitation, thermophoretic precipitation, diffusion and impaction. These samplers collect nanoparticles on a filter, mesh screen or transmission electron microscopy (TEM) grid.

Two broad approaches can be used to collect nanoparticles on grids, *i.e.*, indirect methods and direct methods. Indirect methods have been the usual method used since the 1990s, as in NIOSH Method 7402, Asbestos by TEM (NIOSH 1994). Indirect methods, however, have disadvantages

including particle transfer, labor intensity, and the potential for particle agglomerate changes through the preparation process. The shortcomings of the indirect methods have led scientists to experiment with various methods to directly deposit nanoparticles from the air onto a grid, which is the approach used by the ESP and TPS samplers. Grids can be taken from the collection device and placed directly into a transmission electron microscope for analysis. Two significant disadvantages of the ESP and TSP devices are 1) they are designed to only collect particles with diameters smaller than a micrometer in the nanometer size range, and 2) only some of the particles drawn into each device actually collect on the grid; the rest pass out with the exhaust air.

The sampler described here overcomes both of these shortcomings. A commercial filter cassette installed with an in-house designed and made grid-attached filter has been used (Tsai et al. 2009a) to collect nanoparticles for qualitative identification of nanoparticles. In this device, a filmed TEM grid is taped to the surface of a capillary pore membrane filter and aerosol-laden air is drawn through the filter using a personal sampling pump. Nanoparticles are drawn across the grid by the air flow and a fraction migrate to the filmed grid surface by diffusion; the remaining nanonarticles, and all larger particles entering the device, are collected on the filter. In this study, a new version of the sampling cassette, named Tsai diffusion sampler (TDS), was designed with the novelty of using a specified inlet diameter, cassette housing shape, designed internal height of cassette, and specific airflow to control the cutoff diameter of collected particles so that only respirable particles are sampled. The diffusion mechanism, used for the TDS, is also used by the Naneum wide range aerosol sampler (WRAS) (Gorbunov et al. 2009) and the nanoparticle respiratory deposition (NRD) sampler (Cena et al. 2011); however in these devices the nanoparticles are deposited onto wire meshes or nylon mesh screen rather than TEM grids. With the TDS, the grid collects mostly primary and small agglomerates of submicrometer nanoparticles

via Brownian motion when air flows across the top of the filmed grid. The polycarbonate filter collects particles over a wide size range via diffusion and sieving as air flows through the filter pores, such that many nanoparticles and all of the larger particles are collected on the filter surface between pores.

DESIGN AND METHODS

This TDS is designed to collect particles in the nanometer and respirable size ranges with the aerodynamic cutoff diameter of approximately 3.8 μm for respirable particles. The particle size entering the sampler cassette is determined by a combination of the inlet nozzle size and the sampling air flow. As demonstrated by others (Su and Vincent 2004), the aspiration efficiency of a plain round inlet such as the inlet nozzle at the top of the cassette as shown in Fig. 1a, follows a sigmoidal curve similar to the respirable pre-separator curve. The cutoff diameter of the curve is a function of the inlet diameter and air flow, and must be determined experimentally. The sampler inlet was designed so that the inlet aspiration efficiency is minimally affected by sampling direction (upward, horizontal or downward); this was also reported in the study by Su and Vincent (Su and Vincent 2004). Using the inlet nozzle of a sampling cassette as a pre-separator is also the design principle of the Institute of Medicine (IOM) inhalable mass sampler. By experimentally determining the proper combination of inlet diameter and air flow, the IOM filter cassette aspiration efficiency closely matches the American Conference of Governmental Industrial Hygienists (ACGIH) inhalable mass sampling criterion.

The design approach of the TDS (Fig. 1a) is capable of meeting the performance requirement of a personal sampler that can measure both the nanometer and micrometer portions of the

respirable particles from microscope images; and provide direct sampling and analysis on collected particles using microscopy.

The novel geometry design of the TDS includes 1) 2 mm diameter circular air inlet, 2) 6 mm distance between grid substrate to the inlet opening at the top part of a 25 mm diameter cassette housing (which meets the recommended design criterion of Hinds (Hinds 1999)), 3) smooth curved shape of top cassette housing, to provide smooth air streamline for particle moving from inlet toward the sampling substrate- filter and grid. Together with the design air flow, these factors determine the sizes of particles entering the sampler and thus the cutoff diameter of particles collected on the two substrates. The TDS substrates consist of a 25-mm diameter, 0.22 μm pore size polycarbonate membrane filter (Isopure, Millipore Sigma, Burlington, MA, USA) with a TEM-copper grid in 400 mesh with SiO_2 coated film (SPI, West Chester, PA ,USA) attached to the center of the filter (Fig. 1a). It is operated using a personal sampling pump running at 0.3 L/min air flow (Fig. 2b), pulling particles in the air through the 2 mm diameter circular inlet into the cassette housing. Particles are then collected on both the grid and filter (Fig. 2b).

The sampler was designed using Autodesk Inventor 2018 and 3D printed (ProX 500, 3D Systems, Rock Hill, SC, USA) through selective laser sintering (SLS) of nylon powder. SLS is extremely prevalent in rapid manufacturing practices where it has proven its utility in the automotive and aerospace industries (Zarringhalam et al. 2006). The ProX 500 system used here is able to efficiently manufacture ready to use functioning parts with high resolution and dimensional accuracy (Systems 2017).

Particle Deposition on Grid

As shown in Fig. 1a, a TEM-copper filmed grid was taped onto a 25 mm diameter filter. A metal support screen was used to support the polycarbonate filter. Air was drawn through the filter and aerosol particles deposited on the grid via Brownian diffusion. Theoretically, a particle's diffusion is a function of its diffusion coefficient, D, given by the Stokes-Einstein equation:

$$D = \frac{kTC_c}{3\pi\eta d_p} \quad (1)$$

In this equation, k is Boltzman's constant, T is the absolute temperature, C_c is the Cunningham slip correction factor, η is the gas viscosity, and d_p is the particle diameter.

At standard conditions (constant temperature and viscosity), a particle's diffusion coefficient depends only on its diameter and, as expected, the diffusion increases as the diameter decreases. Since Brownian motion is random, a collection of aerosol particles of the same diameter will be displaced different distances along an arbitrary axis in any given time interval. The distance particles travel under Brownian motion approximates a normal distribution; the root mean square (rms) average distance for a collection of particles' movement in time t by definition is equal to the standard deviation (σ) of the distribution and is given by equation 2 (Hinds 1999).

$$\sigma = X_{rms} = \sqrt{2Dt} \quad (2)$$

Thus, according to Eqs. 1 and 2, during the time t that a particle spends passing the grid, smaller particles can expect to travel a larger average distance than larger ones, so that greater numbers (portion) of smaller particles would be expected to be found on the grid. Thus, nanoparticles, due to their large Brownian displacement, have a high probability of striking a TEM grid element as they pass by the grid; this is illustrated by the following calculations.

At the typical pump air flow of 0.3 L/min through this TDS 25 mm diameter filter cassette (23 mm diameter of filter collecting area), the air flows toward the grid at a velocity of approximately 1 cm/s. Air streamlines striking the center of the grid will be directed toward the edges of the grid;

since the grid has a radius of 1.5 mm, air striking the center of the grid will take approximately 0.15 s to reach the edge. Solving Eqs. 1 and 2, a 10 nm diameter particle, for example, has an rms displacement (X_{rms}) of 0.13 mm in 0.15 s. Since the X_{rms} is also by definition its standard deviation, and 32% of any distribution values are greater than the standard deviation, 32% of the particles will have moved farther than this distance while passing over the grid. Half of these particles will move away from the surface of the grid and half of them (16%) will move toward the surface of the grid and deposit on the filmed opening space of the grid. Thus, 10 nm particles travelling on streamlines that pass within a few tenths of a millimeter of the grid surface will have a high probability of being collected. In addition, flow so close to the surface is likely to be in the frictional boundary layer, meaning that the velocities are lower than the free-stream velocities, the residence times are longer, and more collection by diffusion will occur. The calculated rms displacements range from 0.32 mm for a 4 nm diameter particle to 0.01 mm for a 300 nm diameter particle as shown in Table 1; thus, particles across the entire nanometer size range will have a measurable displacement while passing over the surface of the grid and particles throughout this size range will deposit on the grid due to diffusion.

These calculations indicate that a significant number of the nanometer-sized particles in the air flow impinging on the grid will move to the grid surface and be collected. This particle deposition process has been confirmed experimentally in numerous laboratory and field measurements, described below.

Particle Deposition on Polycarbonate Filter

Particles enter the sampler housing through the inlet probe are distributed onto the filter, and particle agglomerates larger than the pore size (~220 nm) are deposited by sieving. Particles

smaller than the pore size will be deposited onto the filter surface between pores by Brownian motion.

The Nuclepore polycarbonate filter, also known as a membrane filter, has been available since the 1940s, and its properties have been verified (Spurny et al. 1969). The efficiency of diffusion on the membrane filter, E_D, can be calculated by equation 3 (Spurny et al. 1969; Twomey 1962) below when the coefficient of diffusive collection, N_D, shown in equation 4 (Spurny et al. 1969), is greater than 0.01.

$$E_D = 1 - 0.081904 \exp(-3.6568N_D) - 0.09752 \exp(-22.3045N_D) - 0.03248 \exp(-56.95 N_D) - 0.0157 \exp(-107.6N_D) - \ldots \quad (3)$$

The remaining terms in Eq. 3 will approach zero. The coefficient of diffusive collection is given by:

$$N_D = \frac{LDP}{R_0^2 q} \quad (4)$$

Where L is the filter thickness (m), D is the diffusion coefficient (Eq. 1), P is the filter porosity, R_0 is the pore radius of clean filter (m), and q is the face velocity of air at filter (m/s).

For this sampler design, the 0.22 μm porous polycarbonate filter has a thickness of 25 μm (Sigma), porosity of 13.8%, pore radius of 0.11 μm, and q of 0.01 m/s. The diffusion efficiency of the filter is 100% for particles with diameters of 500 nm (0.5 μm) or smaller, and greater than 95% for particles of 1 μm to 0.5 μm as shown in Table 1. Particles with diameters greater than the pore size (220 nm) will of course be collected with 100% efficiency.

The particle's motion entering the sampler inlet and inside the housing, can be characterized using the Stokes number (Stk), Eq. 5 (Hinds 1999). In this equation, τ is the relaxation time (s), calculated using Eq. 6. U_0 is the air velocity, and d_c is the cylinder diameter of airflow which has

been analyzed separately for both the inlet probe diameter (2 mm) and the cassette housing (23 mm) diameter.

$$Stk = \tau \frac{U_0}{d_c} \quad (5)$$

$$\tau = \frac{\rho_p \, d_p^2 \, C_C}{18 \, \eta} \quad (6)$$

Where ρ_p is particle density (kg/m^3).

When Stk >> 1, particles continue moving in a straight line when the air turns; when Stk << 1, particles follow the air streamlines perfectly (Hinds 1999). The particle motion behavior at the probe inlet determines the particle sizes entering the inlet as they follow and deviate from the air streamlines. This determines the maximum size of particles to be sampled by this device, i.e., the largest particle that can follow the sharply-curving streamlines at the device inlet.

Particle Collection and Analysis Protocol

Crystalline aluminum oxide (Al_2O_3) nanopowder (Nanodur, Nanophase, Romeoville IL, USA), with a density of 3600 kg/m^3 and primary particle size of 40 nm, was used as a test aerosol to determine the particle size distribution of collected particles in the TDS. This nanopowder was chosen because of the wide range of aerosol particle sizes from individual primary particles to small and large agglomerates, and the ease of aerosolizing the particles. The experimental setup is illustrated in Fig. 2. Powder was aerosolized inside an ultra-filtered glove box (Terra Universal, Fullerton CA USA, 89 cm x 61 cm x 64 cm) through agitation by stirring 200 mL of aluminum oxide in a container with a compact digital mixer operating at 2000 rotations per minute (rpm) (Cole-Parmer, Vernon Hills IL, USA). The agitator, powder, and sampling cassettes were placed inside the glovebox at center area (Fig. 2), and the aluminum oxide aerosols were diffused to the top opening of the container and pulled into samplers. The air velocity at the sampling area ranged

from 1 to 7.6 cm/s (2 to 15 ft/min) for horizontal direction and from 0 to 3 cm/s (0 to 6 ft/min) for vertical direction.

The glove box and all experimental equipment were decontaminated with clean room wipes and distilled water prior to experimentation. Two direct reading real time instruments (RTIs) were utilized to measure particle number concentrations and size distributions over a range of 10 nm to 10 µm. An Optical Particle Sizer (OPS) (Model 3330, TSI, Shoreview, MN, USA) which measures particles from 0.3 µm to 10 µm, and a Scanning Mobility Particle Sizer (SMPS) (Model 3910, TSI, Shoreview, MN, USA) which has a measuring range of 10 nm to 420 nm collected side by side with one-minute measurement intervals. The RTIs sampled through 1 m of conductive tubing.

The RTIs and three identical TDS samplers were positioned equidistant from each other and 5 cm away in both height and distance from the source (Fig. 2). The RTIs initiated sampling 10 min prior to aerosol generation to establish background concentrations. Directly following this, the three personal sampling pumps and the compact digital mixer were activated. Aerosol generation was conducted for 40 min. Following the sampling period, 10 min of post experimental background was measured with the RTIs.

The RTI data was exported to an Excel spreadsheet where it was analyzed. The TDS TEM grid and filter samples were analyzed with TEM (JOEL JEM-2100F) and scanning electron microcopy (SEM) (JOEL JSL-6500F), respectively. The following TEM imaging protocol was utilized to analyze grid: (1) Five low magnification (50x) images were taken to encompass the entire grid (center, and four quadrants); (2) Four grid spaces were selected equidistant two spaces from the grid center, these spaces were imaged at 500x; (3) The chosen grid spaces were imaged by traversing (9-12 images per grid) the grid space at 5000x until 300 particles were imaged. For filter analysis using SEM, the filters were prepared by cutting a $1/8^{th}$ slice of the filter and coating with

10 nm of gold. Three sections of the filters were imaged (center, middle, and edge) at 9000-25000x until 300 particles were imaged per sample. Particle images were analyzed using FIJI (Schindelin et al. 2012) imaging software to count and measure particle size. The particle sizes were organized following 13 bin ranges within 10 nm to 420 nm and 14 bin ranges above 420 nm to 10 μm, similar to two RTIs bin ranges, to plot particle count frequency with size distribution and cumulative percent particle counts.

RESULTS AND DISCUSSION

The aluminum oxide particles with an average primary size of 40 nm diameter were found to be easily aerosolized and dispersed; they appeared with small primary particles less than 40 nm and agglomerates ranged in nanometer to micrometer sizes. The sampling tests demonstrated a practical exposure scenario where the aerosol concentration varied, with some higher concentrations in some time intervals. The generated aluminum oxide particle concentrations and size distribution were measured throughout the experiment time and presented in Fig. 3a and 3b. The concentration of each size bin and standard deviation data of Fig. 3b are presented in Table S1 (Supplementary Information). Instrument measurements were used to evaluate the particle concentration levels and referenced particle sizes for tests. The size distributions of generated airborne aluminum oxide particles measured by SMPS are shown in the size range from 10 to 420 nm with the mode size measured to be 154 nm. The OPS measurements showed increasing concentrations toward to both minimum and maximum sizes measured by the instrument. The average particle number concentration during 62 min (62 data) of sampling measured by SMPS (10-420 nm) and by OPS (0.3-10 μm) were 237 particles/cm^3 and 7 particles/cm^3, respectively. The peak emission showed concentrations in a range from about 50 to greater than 4000

268 particles/cm^3 for particles smaller than 420 nm; and the particle counts for larger particles above
269 0.3 μm ranged from a few particles to about 80 particles/cm^3. The particle counts were aluminum
270 oxide particles only with essentially 0 particles from the ambient background in the filtered glove
271 box. These emissions represented a low concentration range representative of a typical exposure
272 in none occupational environment.

273 Collected particles on the filter and grid were analyzed separately using SEM and TEM.
274 Typical particle images are presented in Fig. 4. Small particles and agglomerates similar to or
275 smaller than the pore size of filter were collected between pores and/or trapped on pores (Fig. 4a
276 and 4b). Agglomerates were observed as well (Fig. 4a). The TEM grid collected particles on the
277 grid space; many particles were collected on each grid space as seen in Fig. 4c, most of which
278 were primary particles or small agglomerates (Fig. 4d).

279 Numerous images of particles on filter and grid spaces were taken to obtain a minimum of 300
280 particles being counted and analyzed to obtain their sizes. The averages of three sets of sample
281 analyses for particles on filter and grid were calculated. The results are plotted in a cumulative
282 percentile graph versus particle diameters in Fig. 5a. Particles on the filter range in size from 36 to
283 5,800 nm, and particles on grid spaces range in size from 15 to 1,560 nm. The particle mean
284 diameters are 793 nm and 130 nm, respectively, for aluminum oxide particles on the filter and grid
285 spaces.

286 Based on the particle count size distribution, particle characteristics are analyzed and
287 summarized in Table 2. Geometric mean diameter, d_g, was calculated using equation 7 (Hinds
288 1999). Geometric standard deviation, σ_g, was calculated using equation 8 (Hinds 1999).

289 $$\ln d_g = \frac{\sum n_i \ln d_i}{N} \quad (7)$$

290 $$\ln \sigma_g = \left(\frac{\sum n_i (\ln d_i - \ln d_g)^2}{N-1}\right)^{1/2} \quad (8)$$

CMD was obtained from cumulative percentile graph in Fig. 5 at 50% cumulative particle size. CMD was converted to MMD of aluminum oxide particles utilizing the Hatch-Choate conversion equation (Eq 9) (Hinds 1999). The mass median aerodynamic diameter (MMAD) was calculated using Eq. 10 (Hinds 1999).

$$MMD = CMD \exp(3 \ln^2 \sigma_g) \quad (9)$$

$$d_a = d_p (\rho_p/\rho_0)^{1/2} \quad (10)$$

Where d_a is aerodynamic diameter, d_p is particle diameter, ρ_p is particle density, and ρ_0 is standard particle density which is 1 g/cm^3.

For aluminum oxide particles collected on the polycarbonate filter of this sampler, the CMD was 500 nm (0.5 μm) and the MMD was approximately 2 μm. For a lognormal count distribution, d_g is equal to the CMD(Hinds 1999). In Table 2, d_g and CMD differ because the underlying distribution is not actually log-normal as shown in Fig. 5b. The equivalent MMAD of aluminum oxide particles would be approximately 3.8 μm, which is very close to the cutoff diameter of respirable particles (4 μm). The size analysis shown in Fig. 5b when compared to the RTI data in Fig. 3b had smaller particle modes at 65 nm and 116 nm (Fig. 5b) compared to the 154 nm measured by the SMPS. The size range of particles from image analysis extended to above 420 nm, the maximum size measured by SMPS. These two measurements cannot be used to directly compare the absolute sizes of measured particles. The SMPS measured the electrical mobility size of particles, which is correlated with the electrical charge on the surface of three dimensional particles, to determine particle diameter; however, the size analysis of collected particles is based on two-dimensional particle images used to measure the area of imaged individual particles and agglomerates which is then used to calculate the diameter of equivalent spherical particles. The OPS shows increased particle concentration toward to the maximum size of 10 μm in Fig. 3b, but

the TDS is designed to collect particle sizes up to 8 μm aerodynamic diameter so that larger particle agglomerates do not enter the TDS inlet. Thus, differences between these two measurements are expected. Although variations occurred between different measurement approaches, both SMPS and OPS measurements showed that the range of particles collected on filter and grids were also found being detected by both instruments.

A particle's motion while entering the sampler through the inlet probe and inside the sampler housing will vary by its diameter. This relationship can be interpreted using the particle Stokes number as presented in Fig. 6, based on Eq. 5 and data shown in Table S2 (Supplementary Information). When particles enter the inlet probe, aluminum oxide particles approximately 4 μm or smaller will follow the air streamline since the Stokes number is less than 1. For standard-density particles, diameters approximately 8 μm or smaller will follow the air streamline in the inlet probe, since their Stokes number is less than 1. This determines the maximum particle size entering the sampler probe inlet. Once particles enter into the cassette housing, all Stokes numbers are extremely small for particles 10 μm or smaller; thus, all will follow air streamlines.

Contrary to other nanoparticle samplers, quantitative analysis can be performed using the TDS since 100% of the particles entering the sampler are collected on the filter and grid. The particle number concentration can be estimated from the number of particles counted per image, the area of the grid opening that was imaged, the sampling air flow, and the sampling time period to provide a quantitative analysis of size-fractioned particle concentration. This counting protocol is in current development in order to validate the accuracy for various types of particles.

We have further tested this sampler by collecting particles for qualitative analysis in various settings. They include particles emitted from laser printer printing, handling fumed silica powder, disturbing bulk samples of carbon nanotubes, and particles released from mining activity in an

experimental metal mine. Images of such particles collected using the TDS are shown in Fig. 7. The results seen in Fig. 4 demonstrate that the TDS can effectively sample fibrous and non-fibrous particles. Thus, spherical primary particles such as metal, nonmetal or metal-oxide nanoparticles, primary fibrous particles, and agglomerates of all these particles are expected to be collected by the TDS. The theoretical estimation of cutoff diameter for fibrous particles is difficult to estimate due to their high-aspect ratio; the sampler will be further studied experimentally while collecting high-aspect ratio nanoparticles to establish the cutoff particle size and sampling limitations for fibrous particles.

In addition, electrostatic effects of the nonconductive nylon cyclone used for respirable mass sampling has been of concern for its potential to affect particle collection (Almich and Carson 1974). However, the nylon material used in 3D printing the TDS has successfully collected various aerosols, as described above. The sampler material can be altered if required for collecting conductivity-sensitive substances. The TDS can be used for both qualitative and quantitative analysis. The qualitative analysis has also been used by other nanoparticle samplers (Cena et al. 2011; Leith et al. 2014; Miller et al. 2010; Tsai et al. 2012; Tsai et al. 2009a), which identified collected particles' morphology and composition using TEM and energy-dispersive X-ray spectroscopy (EDX). A function has been proposed to quantify collected particles on the TPS (Leith et al. 2014).

Test results to date have shown that the TDS collects nanoparticles at concentrations as low as a few hundred particles per cubic centimeter and thus can be used for short term or long term sampling. The maximum filter loading and pressure drop change when sampling a full work shift will be a subject of further study. The unique features of the TDS is to utilize the design geometry and air flow to determine the cutoff diameter and range of particle sizes entering the sampler, and

the collection of all particles entering the device. Particles entering the TDS will all follow airstream lines and be collected with 100% efficiency, thus allowing for a quantitative analysis of particle concentration and size distribution that is representative of the particle concentration in the sampled air. This sampler is very lightweight with a low sampling air flow and thus is easily used as a typical personal sampling cassette in the field for personal exposure and environmental sampling.

SUPPLEMENTARY INFORMATION

Table S1 and Table S2 are available in Supplementary Information.

ACKNOWLEDGEMENT

Authors acknowledge the financial support of startup fund to Dr. Tsai and patent application by the Colorado State University and financial support to Daniel Theisen's effort by the Centers for Disease Control and Prevention through grant number 5T42OH009229-11. Authors also thank TSI Incorporated for their collaboration and consultation on instrument operation and maintenance.

CONFLICT OF INTEREST

The authors declare that they have no conflict of interest.

FIGURE AND TABLE CAPTIONS

Figure 1. Tsai diffusion sampler (TDS), (a) Illustration of sampler design and components, (b) 3D printed nylon TDS connects to a sampling pump with the grid and filter substrate inside TDS.

Figure 2. Illustration of experimental set up for laboratory particle sampling.

Figure 3. Aluminum oxide particles measured using SMPS and OPS during experiment period (a) Total particle number concentration, (b) Particle size distributions with mode size at 154 nm measured by SMPS.

Note: Average particle total number concentration during 62 min of sampling measured by SMPS (10-420 nm) and by OPS (0.3-10 μm) are 237 particles/cm^3 and 7 particles/cm^3 respectively.

Figure 4: Images of aluminum oxide particles collected on filter and grid. (a) SEM images of particles collected on filter, x20,000; (b) SEM images of particles collected on filter, x60,000; (c) TEM images of particles collected on grid space, x500; (d) TEM images of particles collected on grid space, x5000.

Figure 5. (a) Aluminum oxide particle cumulative size distribution, (b) Aluminum oxide particle count frequency distribution.

Figure 6. Stokes number and corresponded particle diameter for aluminum oxide and standard particles at inlet probe and cassette housing.

Figure 7. TEM images of sampling particles using the TDS. (a) Printer emission particles, (b) Fumed silica particles, (c) Carbon nanotube (CNT), (d) Particles from mining activity.

Table 1: Particles diameters and corresponded parameters including diffusion coefficient (D), coefficient of diffusion collection (N_D), efficiency of collection by diffusion (E_D), and root mean square displacement (X_{rms}).

Table 2: Characteristics of aluminum oxide particles collected on filter and grid.

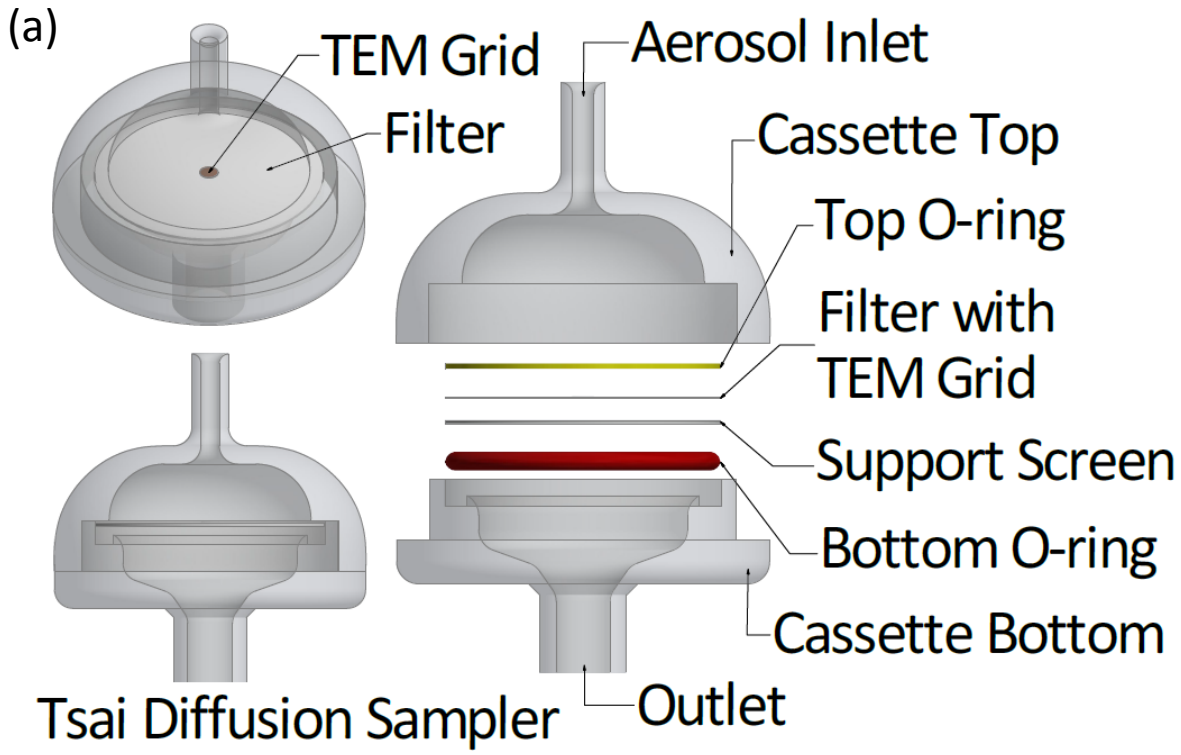

404

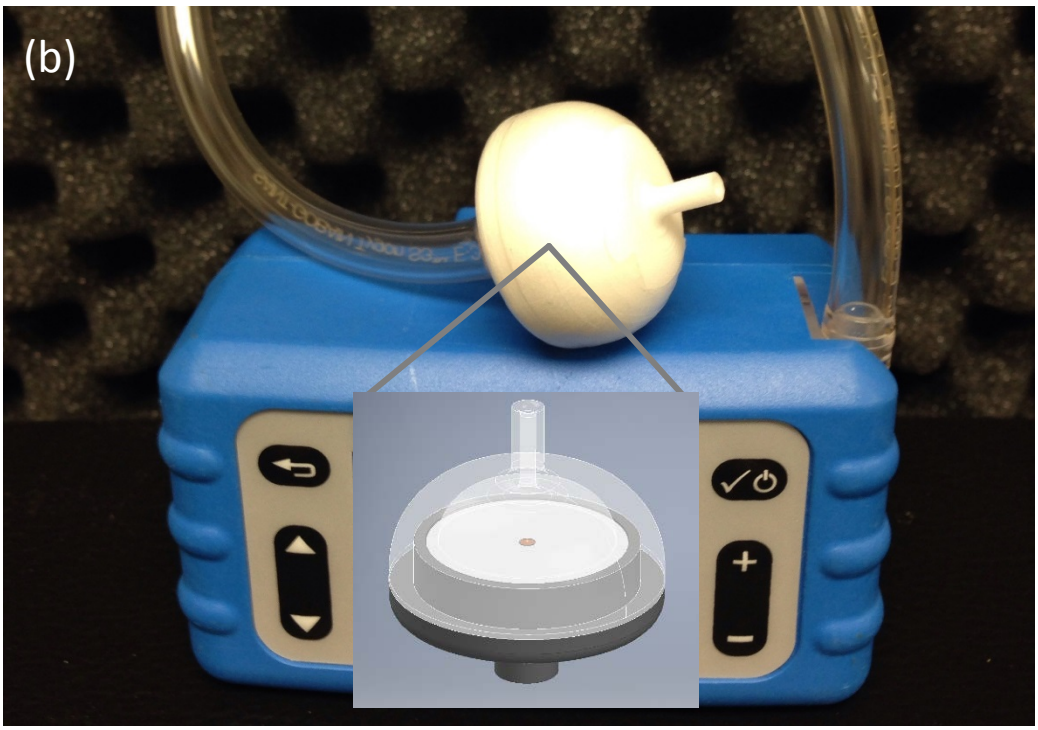

405

406 Figure 1. Tsai diffusion sampler (TDS), (a) Illustration of sampler design and components, (b) 3D

407 printed nylon TDS connects to a sampling pump with the grid and filter substrate inside TDS.

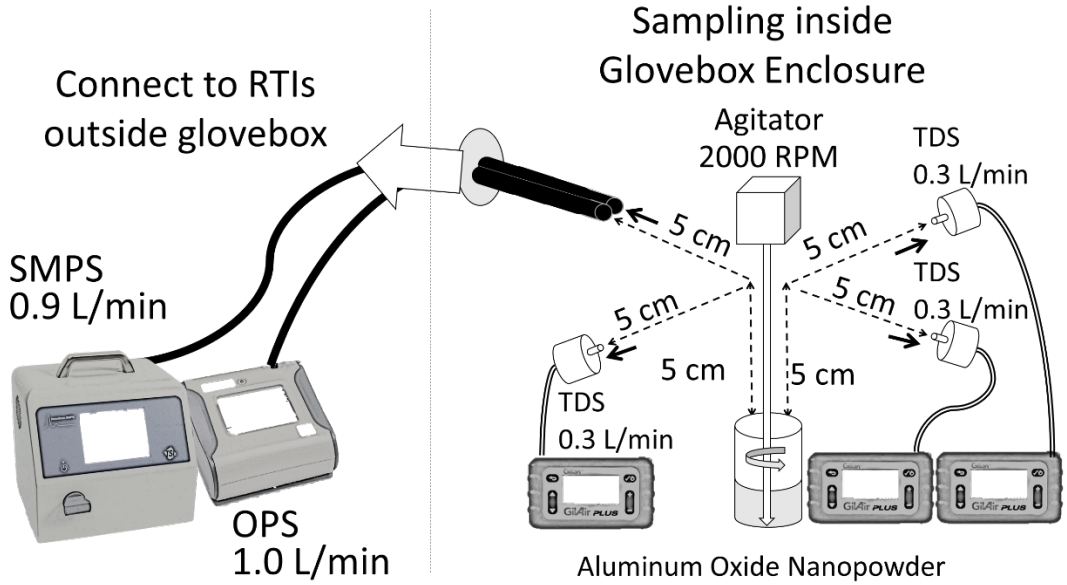

Figure 2. Illustration of experimental set up for laboratory particle sampling

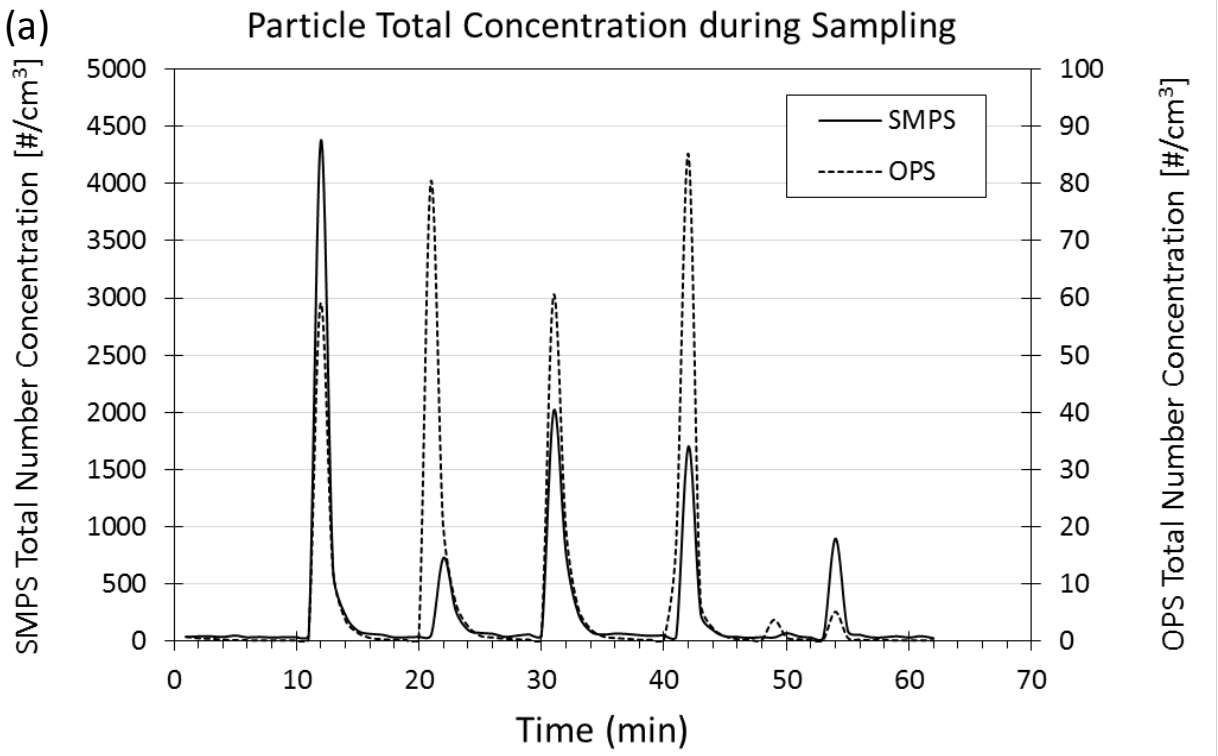
(a)
Particle Total Concentration during Sampling
SMPS Total Number Concentration [#/cm³]
OPS Total Number Concentration [#/cm³]
SMPS
OPS
Time (min)
0
500
1000
1500
2000
2500
3000
3500
4000
4500
5000
0
10
20
30
40
50
60
70
80
90
100
0
10
20
30
40
50
60
70

412

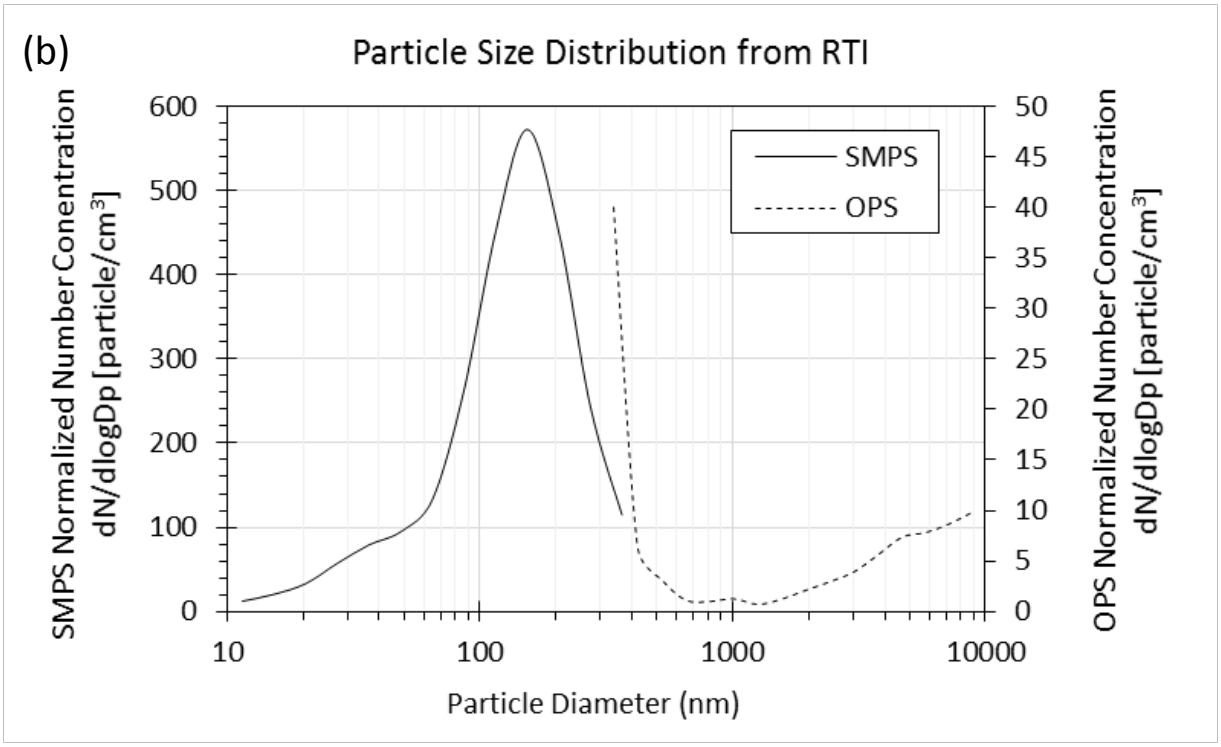
(b)
Particle Size Distribution from RTI
SMPS Normalized Number Conentration dN/dlogDp [particle/cm³]
OPS Normalized Number Concentration dN/dlogDp [particle/cm³]
SMPS
OPS
Particle Diameter (nm)
0
100
200
300
400
500
600
0
5
10
15
20
25
30
35
40
45
50
10
100
1000
10000

413

Figure 3. Aluminum oxide particles measured using SMPS and OPS during experiment period (a) Total particle number concentration, (b) Particle size distributions with mode size at 154 nm measured by SMPS.

Note: Average particle total number concentration during 62 min of sampling measured by SMPS (10-420 nm) and by OPS (0.3-10 μm) are 237 particles/cm^3 and 7 particles/cm^3 respectively.

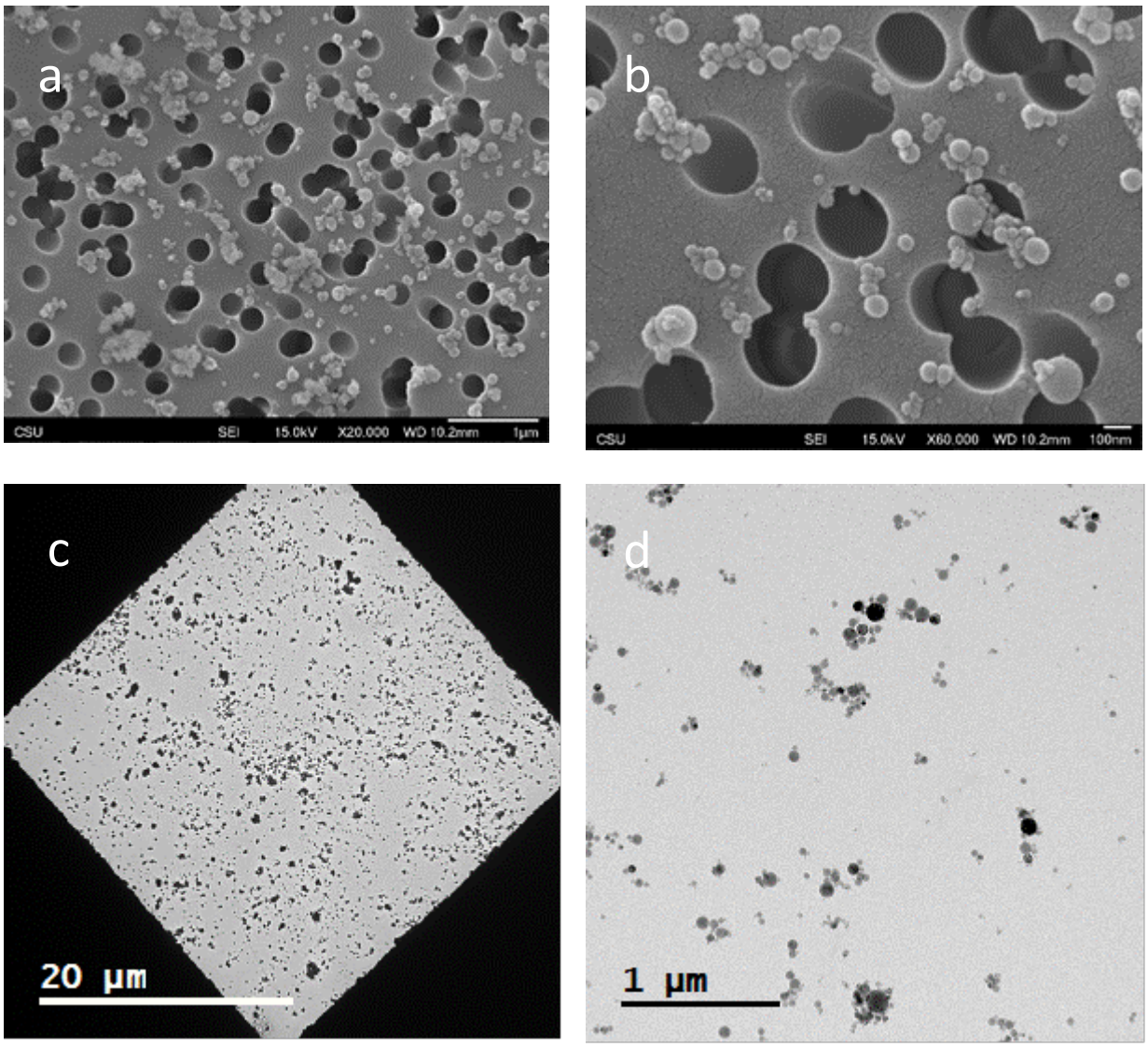

Figure 4: Images of aluminum oxide particles collected on filter and grid. (a) SEM images of particles collected on filter, x20,000; (b) SEM images of particles collected on filter, x60,000; (c) TEM images of particles collected on grid space, x500; (d) TEM images of particles collected on grid space, x5000.

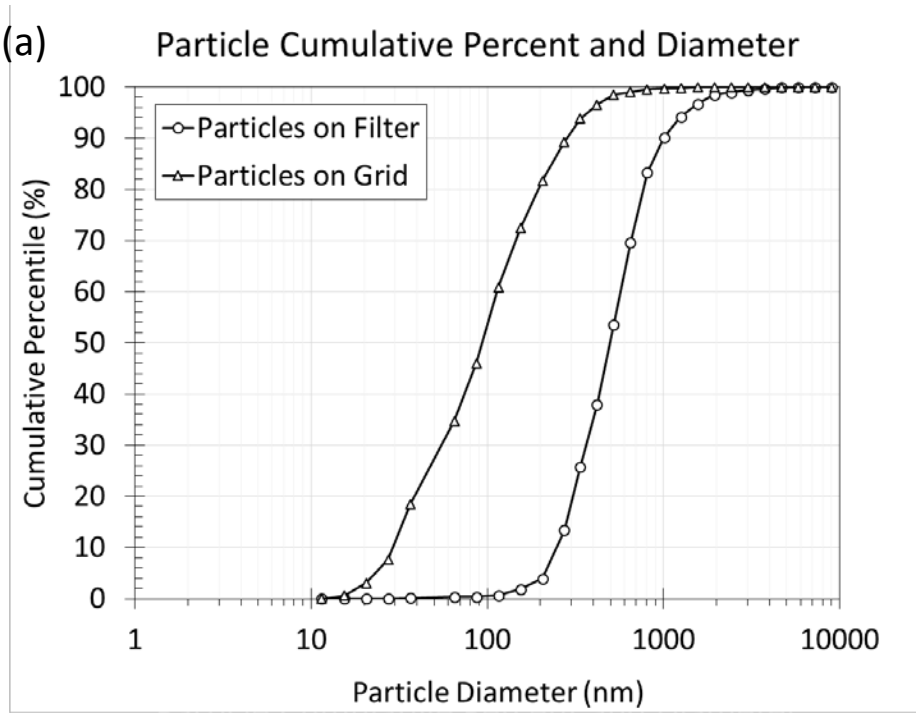

425

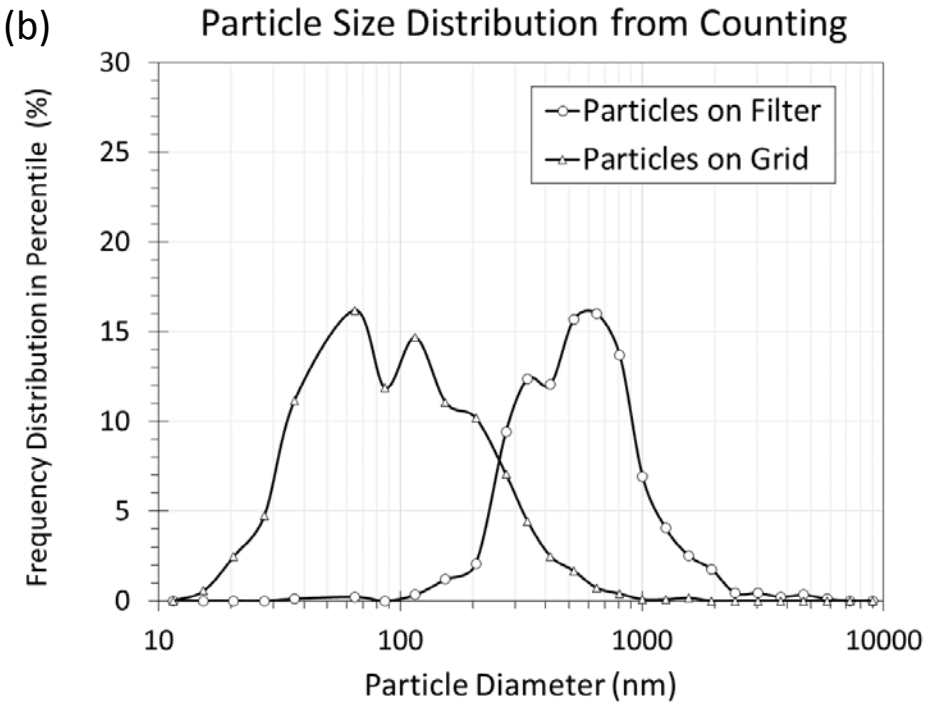

426

427 Figure 5. (a) Aluminum oxide particle cumulative size distribution, (b) Aluminum oxide particle

428 count frequency distribution.

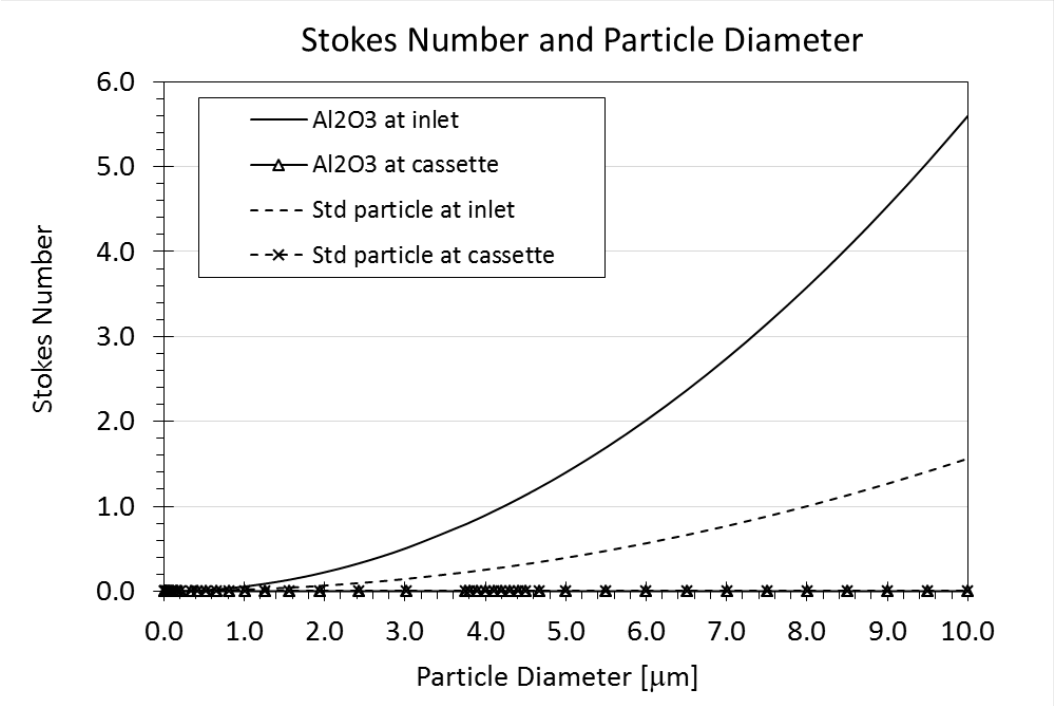

Figure 6. Stokes number and corresponded particle diameter for aluminum oxide and standard particles at inlet probe and cassette housing.

435

(a) Printer emission

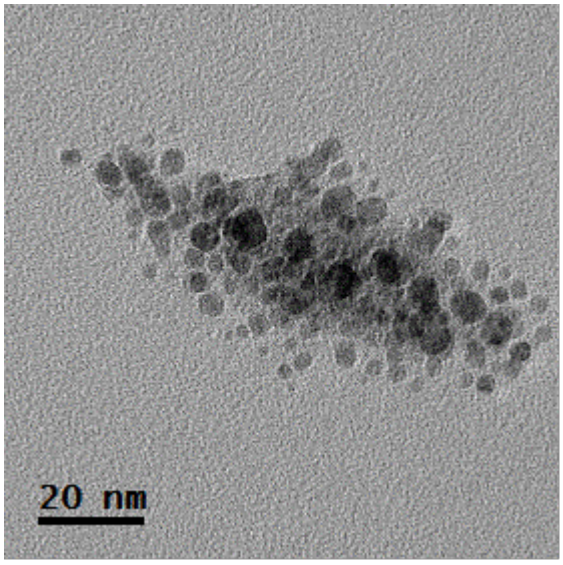

(b) Fumed silica

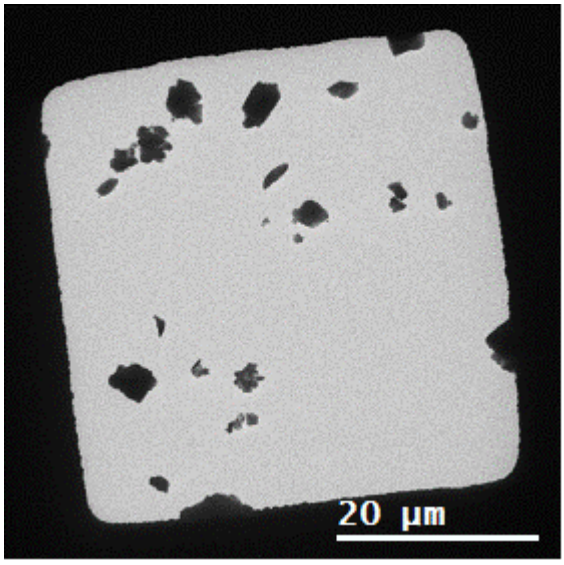

(c) CNT

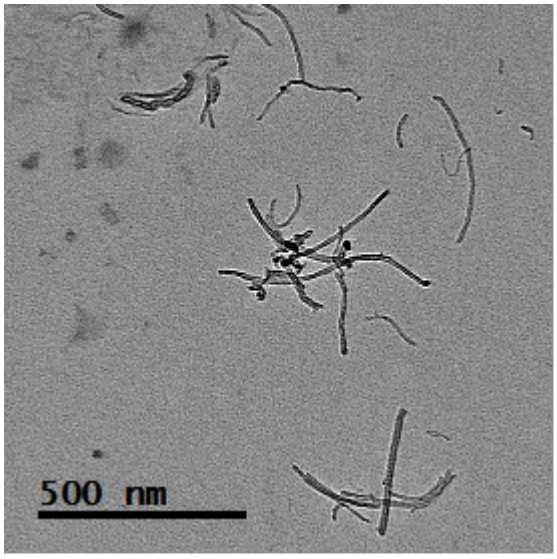

(d) Mine particles

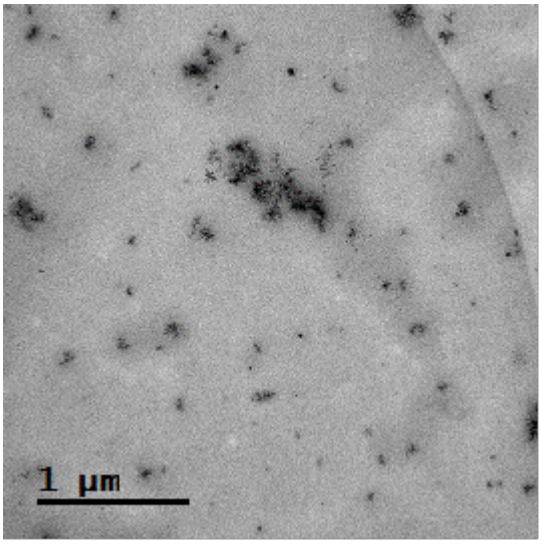

436 Figure 7. TEM images of sampling particles using TDS. (a) Printer emission particles, (b) Fumed

437 silica particles, (c) Carbon nanotube (CNT), (d) Particles from mining activity.

438

439 Table 1: Particle diameters and corresponded parameters including diffusion coefficient (D),
440 coefficient of diffusion collection (N_D), efficiency of diffusion (E_D), and root mean square
441 displacement (X_{rms}).

d (μm)	D (m^2/s)	N_D	E_D	X_{rms} (mm)
0.004	3.35E-07	9377.3	1.00	0.32
0.005	2.15E-07	6018.3	1.00	0.25
0.006	1.5E-07	4198.8	1.00	0.21
0.008	8.46E-08	2368.1	1.00	0.16
0.01	5.45E-08	1525.6	1.00	0.13
0.015	2.45E-08	685.8	1.00	0.09
0.02	1.4E-08	391.9	1.00	0.06
0.03	6.39E-09	178.9	1.00	0.04
0.04	3.69E-09	103.3	1.00	0.03
0.05	2.43E-09	68.0	1.00	0.03
0.06	1.73E-09	48.4	1.00	0.02
0.08	1.03E-09	28.8	1.00	0.02
0.1	6.94E-10	19.4	1.00	0.01
0.15	3.51E-10	9.8	1.00	0.01
0.2	2.23E-10	6.2	1.00	0.01
0.3	1.23E-10	3.4	1.00	0.01
0.4	8.31E-11	2.3	1.00	0.00
0.5	6.24E-11	1.7	1.00	0.00
0.6	4.98E-11	1.4	0.99	0.00
0.8	3.54E-11	1.0	0.98	0.00
1	2.74E-11	0.8	0.95	0.00

442

443

444 Table 2: Characteristics of aluminum oxide particles collected on filter and grid

Al_2O_3 particles	Particles on filter	Particles on grid
Particle mean diameter	793 nm	130 nm
Mean diameter standard deviation	591 nm	127 nm
Geometric mean diameter, d_g	641 nm	92 nm
Geometric standard deviation, σ_g	1.97	2.30
Count median diameter, CMD	500 nm	100 nm
Mass median diameter, MMD	1,987 nm	793 nm
Mass median aerodynamic diameter, MMAD	3,770 nm	1,505 nm

445

446

447

448 **REFERENCES**

449 Almich BP, Carson GA (1974) Some effects of charging on 10-mm nylon cyclone performance.
450 Am Ind Hyg Assoc J 35.

451 Briant JK, Moss OR (1984) The influence of electrostatic charge on the performance of 10-mm
452 nylon cyclones. Am Ind Hyg Assoc J 45(440).

453 Cena L, Peters T (2011) Characterization and control of airborne particles emitted during
454 production of epoxy/carbon nanotube nanocomposites. J Occup Enviro Hyg 8:86-92.

455 Cena LG, Anthony TR, Peters TM (2011) A personal nanoparticle respiratory deposition (NRD)
456 sampler. Enviro Sci Tech 45(15):6483-6490.

457 Dahm MM, Evans DE, Schubauer-Berigan MK, Birch ME, Fernback JE (2012) Occupational
458 exposure assessment in carbon nanotube and nanofiber primary and secondary
459 manufacturers. Ann Occup Hyg 56:542-556.

460 Fleischer T, Grunwald A (2007) Making nanotechnology developments sustainable. A role for
461 technology assessment? J Clean Prod 16:889-898.

462 Gorbunov B, Priest ND, Muir RB, Jackson PR, Gnewuch H (2009) A novel size-selective airborne
463 particle size fractionating instrument for health risk evaluation. Ann Occup Hyg 53(3):225-
464 237.

465 Hinds WC (1999) Aerosol technology - properties, behavior, and measurement of airborne
466 particles. New York: Wiley-Interscience.

467 Leith D, Miller-Lionberg D, Casuccio G, Lersch T, Lentz H, Marchese A, Volckens J (2014)
468 Development of a transfer function for a personal, thermophoretic nanoparticle sampler.
469 Aerosol Sci Technol 48(1):81-89.

470 Maynard AD (2007) Weighing nanotechnology's risks; flying blind. New York Times.

471 Methner MM, Birch ME, Evans DE, Ku BK, Crouch K, Hoover MD (2007) Case Study:
472 identification and characterization of potential sources of worker exposure to carbon
473 nanofibers during polymer composite laboratory operations. J Occup Enviro Hyg
474 4(12):D125-30.
475 Miller A, Frey G, King G, Sunderman C (2010) A handheld electrostatic precipitator for sampling
476 airborne particles and nanoparticles. Aerosol Sci Technol 44(6):417-427.
477 NIOSH (1994) Asbestos by TEM. Cincinnati, OH: Department of Health and Human Services,
478 Centers for Disease Control and Prevention, National Institute for Occupational Safety and
479 Health.
480 NSTC (2006) Environmental, health, and safety research needs for engineered nanoscale materials.
481 Washington, D.C.: National Science and Technology Council (NSTC), the National
482 Nanotechnology Initiative, Executive Office of the President of the United States.
483 Oberdörster E (2004) Manufactured nanomaterials (fullerenes, C60) induce oxidative stress in the
484 brain of juvenile largemouth bass. Enviro Health Persp 112(10):1058-1062.
485 Park J, Kwak BK, Bae E, Lee J, Kim Y, Choi K, Yi J (2009) Characterization of exposure to silver
486 nanoparticles in a manufacturing facility. J Nanopart Res 11(7):1705-1712.
487 Roco MC (2003) Broader societal issues of nanotechnology. J Nanoparticle Res 5:181-189.
488 Roco MC (2011) Erratum to: The long view of nanotechnology development: the National
489 Nanotechnology Initiative at 10 years. J Nanoparticle Res 13:1335-1335.
490 Schindelin J, Arganda-Carreras I, Frise E, Kaynig V, Longair M, Pietzsch T, Preibisch S, Rueden
491 C, Saalfeld S, Schmid B (2012) Fiji: an open-source platform for biological-image analysis.
492 Nature methods 9(7):676-682.

493 Schulte P, Geraci C, Zumwalde R, Hoover M, Castranova V, Kuempel E, Murashov V, Vainio H,
494 Savolainen K (2008) Sharpening the focus on occupational safety and health in
495 nanotechnology. Scandinavian J Work Enviro Health 34(6):407-409.
496 Sigma M. GTTP02500 Isopore Membrane Filter. accessed on Jan. 2018
497 http://www.emdmillipore.com/US/en/product/Isopore-Membrane-Filter,MM_NF-
498 GTTP02500.
499 Simeonova PP, Opopol N, Luster MI (2007) Nanotechnology--toxicological issues and
500 environmental safety. Dordrecht, Netheralnds: Springer. 276 p.
501 Singh S, Nalwa HS (2007) Nanotechnology and health safety--toxicity and risk assessments of
502 nanostructured materials on human health. Journal of nanoscience and nanotechnology
503 7(9):3048-3070.
504 Spurny K, Lodge J, Frank E, Sheesley D (1969) Aerosol filtration by means of nuclepore filters
505 structural and filtration properties. Enviro Sci Tech 3(5).
506 Su W-C, Vincent JH (2004) Experimental measurements and numerical calculations of aspiration
507 efficiency for cylindrical thin-walled aerosol samplers in perfectly calm air. Aerosol Sci
508 Technol 38(8).
509 Systems D (2017) ProX SLS 500. Retrieved from: https://www.3dsystems.com/3d-printers/prox-
510 sls-500.
511 Tsai CJ, Liu CN, Hung SM, Chen SC, Uang SN, Cheng YS, Zhou Y (2012) Novel active personal
512 nanoparticle sampler for the exposure assessment of nanoparticles in workplaces. Environ
513 Sci Technol 46(8):4546-4552.
514 Tsai SJ (2013) Potential inhalation exposure and containment efficiency when using hoods for
515 handling nanoparticles. J Nanopart Res 15:1880.

516 Tsai SJ, Ada E, Isaacs J, Ellenbecker MJ (2009a) Airborne nanoparticle exposures associated with
517 the manual handling of nanoalumina and nanosilver in fume hoods. J Nanopart Res
518 11(1):147-161.
519 Tsai SJ, Ashter A, Ada E, Mead J, Barry C, Ellenbecker MJ (2008) Airborne nanoparticle release
520 associated with the compounding of nanocomposites using nanoalumina as fillers. Aerosol
521 Air Quality Res 8(2):160-177.
522 Tsai SJ, Hofmann M, Hallock M, Ada E, Kong J, Ellenbecker MJ (2009b). Characterization and
523 evaluation of nanoparticle release during the synthesis of single-walled and multi-walled
524 carbon nanotubes by chemical vapor deposition. Environ Sci Technol 43(15):6017-6023.
525 Tsai SJ, Huang RF, Ellenbecker MJ (2010) Airborne nanoparticle exposures while using constant-
526 flow, constant-velocity, and air-curtain-isolated fume hoods. Ann Occup Hyg 54(1):78-87.
527 Twomey S (1962) Equations for the decay of diffusion of particles in an aerosol flowing through
528 circular and rectangular channels. Bull Obs Puy de Dome 10.
529 Warheit DB, Sayes CM, Reed KL, Swain KA (2008) Health effects related to nanoparticle
530 exposures: environmental, health and safety considerations for assessing hazards and risks.
531 Pharmacology & Therapeutics 120(1):35-42.
532 Zarringhalam H, Hopkinson N, Kamperman NF, De Vlieger JJ (2006) Effects of processing on
533 microstructure and properties of SLS Nylon 12. Materials Sci Eng A(435).